Time analysis of above-threshold ionization in extreme-ultraviolet laser pulses

H. Ebadi, C. H. Keitel, and K. Z. Hatsagortsyan*
Max-Planck-Institut für Kernphysik, Saupfercheckweg 1, D-69117 Heidelberg, Germany
(Received 11 February 2011; published 27 June 2011)

The strong field ionization dynamics of an atom in a strong extreme-ultraviolet radiation field is investigated using numerical solutions of the time-dependent Schrödinger equation. The analysis of the electron quantum distribution in phase space after the interaction provides detailed information on the ionization time evolution. It evidences the interrelation among the periodic slow drift of the bound electron wave packet in the highly oscillating field, the modulation of the ionization wave packet, and the previously unknown fine structure of above-threshold ionization spectra in the stabilization regime.

DOI: 10.1103/PhysRevA.83.063418 PACS number(s): 32.80.Rm, 32.80.Fb

I. INTRODUCTION

The laser technique is advancing rapidly into the short-wavelength domain. Tabletop radiation sources based on high-order harmonic generation provide strong coherent radiation in the extreme-ultraviolet (XUV) domain [1]. Stronger fields ranging from XUV to the soft x-ray regime are produced by large-scale free electron lasers such as the Free-electron LASer in Hamburg (FLASH), Germany, Linac Coherent Light Source (LCLS) in Stanford, USA, and Spring-8 Compact SASE Source (SCSS) in Japan [2]. Although the current FLASH intensities are in the perturbative multiphoton regime [3], the generation of higher intensities are anticipated in the near future [4], which will open up opportunities for experimental investigation of nonperturbative strong field atomic phenomena at high frequencies. Recently, great attention has been devoted to the investigation of specific features of multiphoton ionization in strong XUV laser fields, in particular, to above-threshold ionization (ATI) [5,6], multiple ionization [7,8], many-electron effects in multiphoton ionization [9], and angular distribution of photoelectrons at high frequencies [10].

It is well known that in the high-frequency limit when $\omega \gtrsim I_p$ (atomic units are used throughout the paper), where ω is the laser frequency and I_p is the atomic ionization potential, stabilization of atoms against ionization can happen in a rather intense laser field [11]. The formalism of high-frequency Floquet theory (HFFT) has been developed to explain this phenomenon in a monochromatic laser field (quasistationary stabilization) [12], according to which the stabilization is due to the formation of electron quasistationary states in the atomic potential averaged over the fast electron oscillations in a laser field (Kramers-Henneberger (KH) potential [13]). On the other hand, direct integration of the time-dependent Schrödinger equation (TDSE) has been used to study nonadiabatic effects for the stabilization in a pulsed laser field (dynamic stabilization) [14,15]. Though the stabilization phenomenon was discovered and explained about 20 years ago, the interest in this regime has been renewed recently. Thus, a recent study of HFFT by Gavrila [16] indicates that atomic stabilization can be established even at laser frequencies lower than the atomic frequency, namely at $\omega\alpha^{2/3} \gg 1$ [17], where $\alpha = E_0/\omega^2$ is the classical excursion amplitude of the electron in a laser field and E_0 is the amplitude of the laser field. Further, a unified view of low- and high-frequency regimes has been proposed in [18]. Fine structures in high-order harmonic generation spectra in the stabilization regime due to hyper-Raman transitions have been shown in [19]. Fine features of ATI spectra in the dynamic stabilization regime are reported in Refs. [20] and [21]. In particular, in this situation, a single ATI spectral line acquires a structure due to interference of ionization waves emitted at the rising and falling edges of a laser pulse. The adiabatic variation of the envelope of the laser pulse is shown to be responsible for the appearance of a low-energy continuous structure.

The aim of this paper is to investigate the details of time evolution of the ionization dynamics in a strong XUV field via analysis of the electron distribution in quantum phase space after the interaction. We show that the periodic slow drift of the bound electron wave packet (WP) under the action of the highly oscillating laser and Coulomb fields produces modulation of the ionization WP. The latter is directly related to a previously unknown fine structure in ATI spectra in the stabilization regime. The reason for such an interference structure is shown to originate from the interference of multiple paths to the continuum via different intermediate bound states.

The structure of the paper is as follows. In Sec. II, the theoretical model is introduced. The results of the time analysis of the ionization dynamics are presented in Sec. III. The fine structures of spectral lines are discussed in Sec. IV. The case of low-frequency stabilization is briefly discussed in Sec. V, and the conclusion is formulated in Sec. VI.

II. THEORETICAL MODEL

We describe the electron dynamics in a strong XUV laser field by the Schrödinger equation in the dipole approximation:

$$i\frac{\partial}{\partial t}\Psi(x,t) = \left\{\frac{1}{2}\left(\hat{p}_x - \frac{A(t)}{c}\right)^2 + V(x)\right\}\Psi(x,t). \qquad (1)$$

This is justified up to a laser field strength of $E_0 \lesssim 80$ a.u. at $\omega = 3$ a.u. according to the condition $c\xi^2/2\omega \lesssim a_b$ for neglecting relativistic effects [22,23], with the bound electron WP size a_b, the laser field parameter $\xi = E_0/c\omega$, and the speed of light c. Here, $V(x) = -e^{-x^2/R^2}/\sqrt{a^2+x^2}$ is the potential of a one-dimensional (1D) model atom with a soft-core parameter $a = 1.4$ a.u. chosen to fit the ionization potential of a hydrogen atom, R is the range of the atomic potential ($R \to \infty$, if not

*k.hatsagortsyan@mpi-k.de

specified otherwise), and $E(t) = -A'(t)/c = E_0 f(t)\cos\omega t$ is the laser pulse. The laser pulse envelope $f(t)$ is trapezoidal with an overall duration t_d:

$$f(t) = \begin{cases} \sin^2(\pi t/2t_{\rm on}) & 0 < t < t_{\rm on} \\ 1 & t_{\rm on} < t < t_{\rm off} \\ \sin^2[\pi(t_{\rm d} - t)/2t_{\rm on}] & t_{\rm off} < t < t_{\rm d}. \end{cases} \quad (2)$$

In order to avoid reflection of the WP at the boundaries, a negative imaginary potential is used. The TDSE is solved numerically by a direct integration method [24] using an appropriate split-operator technique and the Crank-Nicolson finite-difference scheme [25]. Based on the results of [15], we can state that our 1D calculations provide a qualitative description of the involved stabilization dynamics as compared to those obtainable from a more realistic three-dimensional (3D) model. The ATI spectra and its time profile in different regions are calculated by applying the window operator $\hat{W}(\varepsilon,n,\sigma)$ to the final wave function $|\Psi_f\rangle$:

$$\hat{W}(\varepsilon,n,\sigma) = \frac{\sigma^{2^n}}{(\hat{H}_0 - \varepsilon)^{2^n} + \sigma^{2^n}}, \quad (3)$$

where $\hat{H}_0$ is the field-free Hamiltonian, ε is the energy of the extracted wave function, 2σ is the energy bandwidth of the extraction, and the parameter n defines the sharpness of the energy window [26]. The probability that the electron after the interaction has an energy ε within a bandwidth of 2σ is given by

$$\rho_\sigma(\varepsilon) = \langle\Psi_f|\hat{W}^2(\varepsilon,n,\sigma)|\Psi_f\rangle = \int dx\, \rho_\sigma(\varepsilon,x). \quad (4)$$

We interpret the distribution function $\rho_\sigma(\varepsilon,x)$ as a quantum phase-space distribution (in energy and position space), following [27]. It is similar to the Husimi phase-space distribution but has an advantage in resolution. To visualize a small structure in the ionized electron WP, a rather small energy bandwidth σ of the distribution function should be applied. In fact, due to a finite-energy bandwidth, the electron momentum p has an uncertainty $\delta p \sim 2\sigma/p$, which brings an uncertainty for the coordinate during the time $\delta t \sim x/p$: $\delta x \sim p\delta p\delta t \sim \sigma x/\varepsilon$. Any structure in the phase space with a characteristic size $(\Delta x, \Delta p)$ will be visible if $\delta x \ll \Delta x$ and $\delta p \ll \Delta p$. These conditions yield $\sigma/\varepsilon \ll \Delta x/x$ and $\sigma/\varepsilon \ll \Delta p/p$. If the laser pulse consists of N cycles and the time structure to be resolved consists of ΔN cycles, the first of the above conditions reads

$$\frac{\sigma}{\varepsilon} \ll \frac{\Delta N}{N}. \quad (5)$$

In particular, the electron quantum orbits (the localized contribution to the ionized electron WP within one laser period, $\Delta N = 1$) will be resolved at $\varepsilon \gg N\sigma$. Additionally, the requirement of the uncertainty relation $2\pi/\delta p \ll \Delta x$ restricts σ from below:

$$\Delta N 2\sigma \gg \omega. \quad (6)$$

To single out the signatures of the classical dynamics in the quantum case, we have carried out also classical trajectory Monte Carlo (CTMC) simulations and compared them with the quantum results.

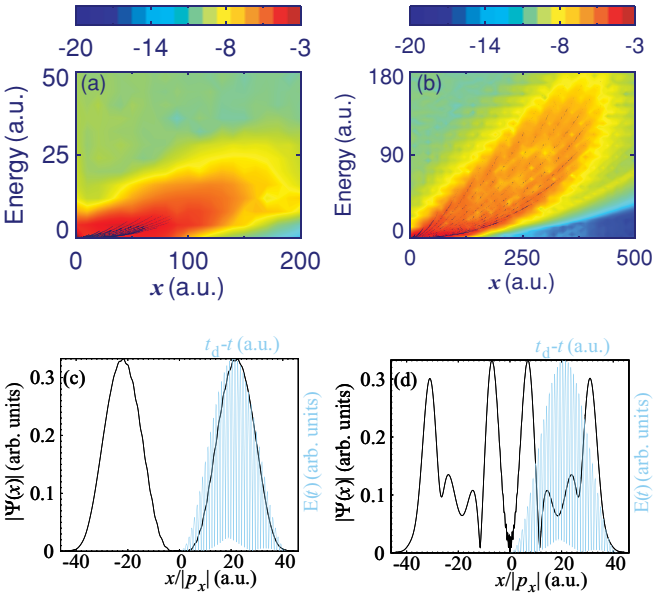

FIG. 1. (Color online) The quantum phase-space distribution of the ionized electron WP after the interaction with a laser pulse of frequency $\omega = 3.0$ a.u.: (a) and (c) in the perturbative regime, with the peak electric field $E_0 = 4$ a.u., (b) and (d) in the stabilization regime, with the peak electric field $E_0 = 25$ a.u.. The black lines in (a) and (b) indicate the classical trajectories, which are launched with initial zero momentum at moments when the field is at maximum and later are driven only by the laser field. Panels (c) and (d) show the time profile of the ionization probability (cut across the phase space) at $\varepsilon = 2\omega$. $\sigma = 2$ a.u. in (a) and (b) and $\sigma = 1$ a.u. in (c) and (d). The laser pulse is shown in (c) and (d) with a blue (grey) line consisting of 20 optical cycles.

III. TIME ANALYSIS OF THE IONIZATION DYNAMICS

Examples of the quantum phase-space distribution (the probability distribution over the electron coordinate and energy after the interaction) below and above stabilization regime are shown in Figs. 1 and 2. The high-frequency case ($\omega > I_p$) is shown in Fig. 1, and the low-frequency case ($\omega < I_p$) appears in Fig. 2. The stabilization regime is determined according to the dependence of the ionization probability on the laser intensity; see Fig. 3.

Below stabilization, there is a uniform contribution into the ionization WP from each cycle of the laser field; see Fig. 1(a). In the stabilization regime, the contribution to the ionization WP is localized in each laser period [see Fig. 1(b)], giving rise to quantum orbits in the phase space at high electron energies [in this case $\Delta N = 1$ and $\sigma = 2$ a.u. have been chosen to fulfill Eq. (6) in Figs. 1(a) and 1(b)]. In Figs. 1(a) and 1(b), the classical trajectories for the ionized electrons are shown in black. The latter are launched with initial zero momentum at a moment when the field is at maximum and latter is driven only by the laser field. Note that in the stabilization regime there is a good correspondence of the quantum orbits to the classical ones. At low electron energies, single quantum trajectories are not resolved [see the conditions in Eqs. (5) and (6)], but still resolving longer structures are possible. Thus, at the electron energy $\varepsilon = 2\omega$, structures longer than 3.5 laser periods can be resolved using $\sigma = 1$

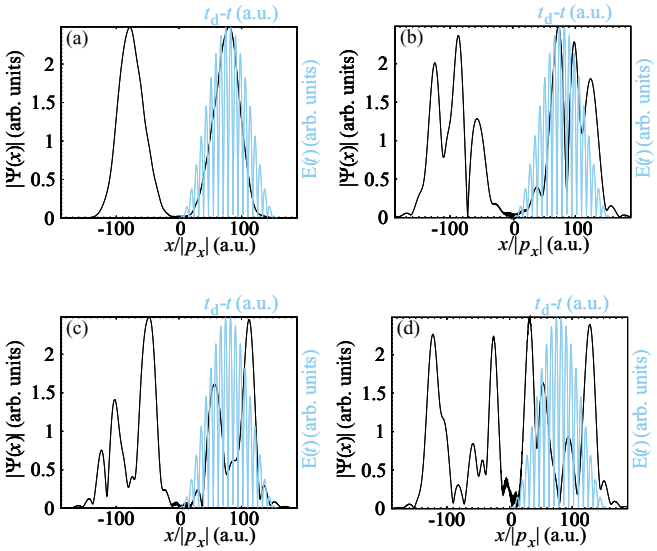

FIG. 2. (Color online) The time profile of the ionization probability of the electron WP at $\varepsilon = 2$ a.u. with $\sigma = 0.3$ a.u.. The peak electric field is (a) $E_0 = 0.16$ a.u., (b) $E_0 = 0.64$ a.u., (c) $E_0 = 1.28$ a.u., and (d) $E_0 = 2.88$ a.u., and the laser frequency $\omega = 0.4$ a.u.. The laser pulse is shown with a blue (grey) line consisting of 10 optical cycles.

a.u. bandwidth. For analysis of details of the phase-space distribution, we use a cut across the phase-space distribution at a certain energy with an energy bandwidth of 2σ a.u.. The latter, with an appropriate coordinate-to-time mapping $t = x/\sqrt{2\varepsilon}$, provides the time profile of the ionization WP at a given electron energy; see Figs. 1(c) and 1(d). Below the stabilization, the ionization WP follows the envelop of the laser pulse, which indicates the prevailing of one photon process: the instantaneous ionization probability is proportional to the laser intensity; see Figs. 1(c) and 2(a). At high intensities, the two-peak structure is indicative of the stabilization regime; see Figs. 1(d) and 2(d). The ionization probability is suppressed at the pulse maximum due to the stabilization, and the ionization is enhanced only at the rising and the lowering edges of the laser pulse. We observe also intermediate peaks between the

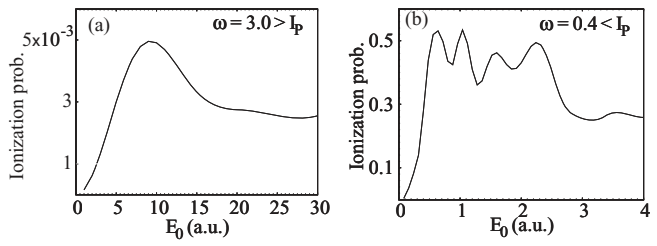

FIG. 3. To choose an appropriate laser intensity, the ionization probability of a 1D hydrogen atom as a function of the electric field of the laser pulse is shown: (a) $\omega = 3$ a.u. and (b) $\omega = 0.4$ a.u.. The laser pulse is of $\sin^2$ form with zero flat duration and consists of $N = 20$ cycles. The ionization probability is calculated by projecting out the bound states at the end of the pulse. The stabilization regime is characterized by a constant (low-frequency) or decreasing (high-frequency) ionization probability with increasing the laser intensity.

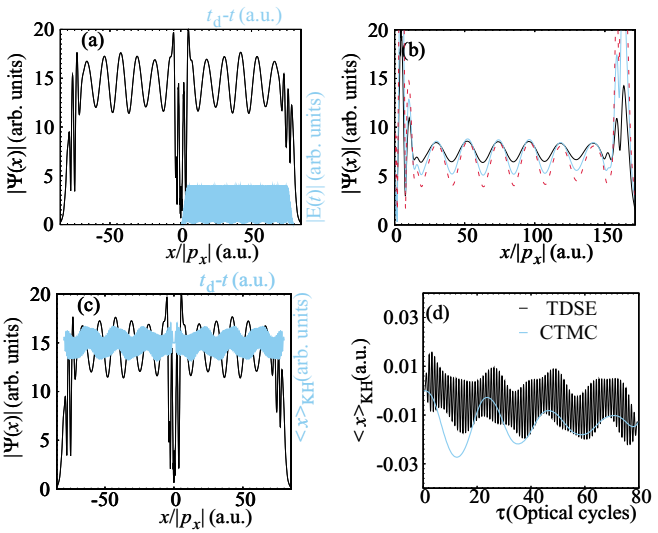

FIG. 4. (Color online) The time profile of the ionization WP after the interaction with an 80-cycle laser pulse including 5-cycle ramp, $\omega = 3$, $E_0 = 25$, and $\sigma = 1$. The atomic potential is modeled by a short range potential: (a) the electron energy $\varepsilon = 4\omega$ [the laser pulse is shown with a blue (grey) line] and (b) (black line) $\varepsilon = 4\omega$, (dashed red line) $\varepsilon = 5\omega$, and (blue/grey line) $\varepsilon = 6\omega$. (c) The time profile of the ionization WP from (a) is superimposed by the expectation value of the electron displacement (blue/grey line) from (d). (d) The expectation values of the electron displacement according to TDSE (black line) and CTMC (blue/grey line).

major ionization bursts, arising during the flat part of the laser pulse, which we will look more closely further.

At low frequencies, there are characteristic differences in the phase-space structure. First, left-right asymmetry exists, which arises due to a large electron drift on the rising ramp of the laser pulse at low energies; see Figs. 2(b) and 2(c). Second, the intermediate structures are more prominent, the reason of which could be the repopulation of the excited states due to resonances.

The intermediate structures appear more regular in the case of a rather long laser pulse. Therefore, we consider the ionization process in a laser pulse consisting of 80 cycles with 70-cycle constant amplitude. The time profile of the photoelectron WP with a certain energy in this case is shown in Fig. 4. The ionization WP is modulated, as one can see from Fig. 4(a). Moreover, the modulation phase is the same at different electron energies [see Fig. 4(b)], which means that the total ionization yield is periodically enhanced during the interaction. The characteristic time scale of this periodic enhancement is much larger than the laser period. This hints at the possible connection of the ionization enhancement with the slow drift of the electron classical trajectory in the KH potential. It is known that in a laser field the electron drifts along the laser polarization direction with a uniform velocity, besides its oscillation with the laser frequency. In the case of an atom in a strong laser field of high frequency, the drift of the electron is not uniform due to the influence of the Coulomb field of the atomic core. In particular, the direction of the drift changes to its opposite when the turning point of the electron fast oscillation approaches the core [28]. Near the turning point, the electron velocity is small. Because of that, when the

turning point is close to the nucleus, the interaction time of the electron with the core is relatively large, which allows a large momentum transfer to the electron from the core, fostering the photon absorption and the electron transition to the continuum. Therefore, at this point, the ionization probability can be enhanced. To check this hypothesis, we have calculated the quantum expectation value of the electron coordinate via TDSE solution as well as the average coordinate according to the CTMC simulation; see Fig. 4(c). The average value of the electron displacement from the CTMC and TDSE calculations are qualitatively consistent. Moreover, the maxima of oscillations in the time profile of the ionized WP correspond to the turning points of the electron displacement $\langle x(t)\rangle_{\rm KH}$ [see Fig. 4(d)], which supports our assumption that the Coulomb field influence at the turning points of the drift enhances the ionization probability. In the next section, we investigate the implication of a then more significant drift of the bound electron WP on the ionization spectra.

IV. IONIZATION SPECTRA

Let us to investigate the ATI spectrum for a model atom with a short-range potential. In this model, a finite number of bound states exists, which simplifies the analysis of the role of excited bound states in the ionization dynamics. The spectrum of the ionized WP with one- and four-photon absorption for the model atom with four field-free states is shown in Fig. 5. The two peaks in the spectral line result from the photoionization of the ground and the second excited KH light-induced states, while the deep position between the peaks corresponds to the absorption of four photons from the first excited KH state [29]. The ionization from the other bound states are at the level of the background. One can see a good correlation between the time profile of the ionized WP in Fig. 4(a) and the electron spectrum in Fig. 5. According to the spectrum, the ionized WP of a certain energy ε (with a bandwidth $2\sigma = 2$) is formed from the contributions which originate either from the ground state or from the second excited state: $\psi_\varepsilon = a_1 \exp(ip_1 x - i\varepsilon_1 t) + a_2 \exp(ip_2 x - i\varepsilon_2 t)$, where $\varepsilon_{1,2} = \varepsilon_{g,e_2} + n\omega$, n is the number of absorbed photons, $p_{1,2} = \sqrt{2\varepsilon_{1,2}}$, and ε_{g,e_2} is the energy of the ground or the second excited state, respectively. Consequently, the density of the ionized WP at the energy ε is modulated by a frequency corresponding to the energy difference $\varepsilon_{e_2} - \varepsilon_g$:

$$|\psi_\varepsilon|^2 = |a_1|^2 + |a_2|^2 + 2|a_1||a_2|\cos(\Delta p x - \Delta\varepsilon t + \Delta\varphi), \tag{7}$$

where $\Delta\varphi = \arg\{a_1^* a_2\}$. The modulation length is $\Delta x = 2\pi/\Delta p = 2\pi p/\Delta\varepsilon$, and the modulation period is $\Delta t = \Delta x/p = 2\pi/\Delta\varepsilon$, or expressed via the number of laser cycles $\Delta N = \Delta t/T = \Omega\Delta\epsilon$, with the laser period $T = 2\pi/\omega$. From the spectrum of Fig. 5, $\omega/\Delta\varepsilon \approx 10.6$, which approximately corresponds to the modulation duration in Fig. 4(a), which is $\Delta N \approx 11.3$. In other words, when the ionization WP is modulated with a period Δt, then the spectrum should contain not only harmonics of the photon energy but also satellites $n\omega + k\Omega$, with $\Omega = 2\pi/\Delta t$. The second peak in the spectral line, in fact, fits to the position of the satellite with $k = 1$.

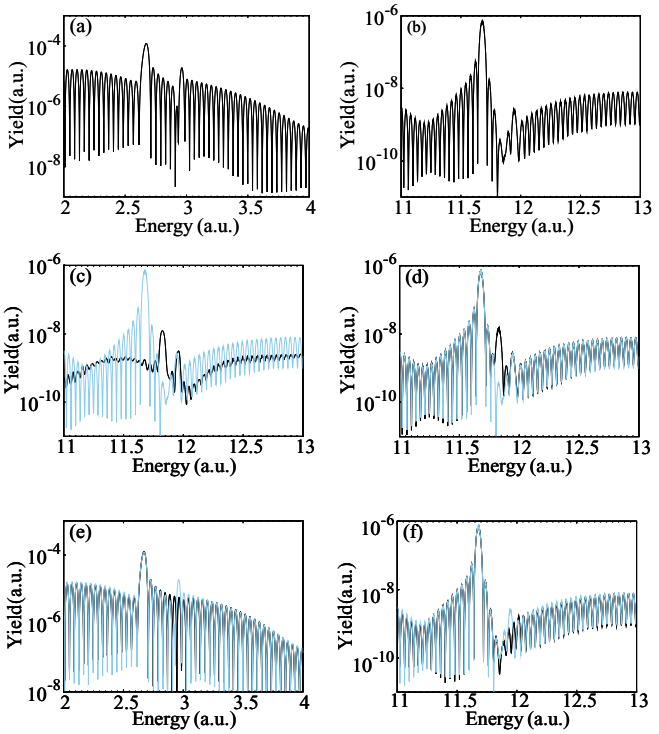

FIG. 5. (Color online) ATI spectra for the same system as in Fig. 4: in the energy range over (a) 2–4 a.u. and (b) 11–13 a.u.. In (c), the first KH state is projected out after the laser pulse ramp, in (d) the second KH state is projected out after the ramp, and in (e) and (f) the third KH state after the ramp is projected out with (e) one photon ionization and (f) four photon ionization. The spectrum of panel (b) is repeated in (c), (d), and (f) and the spectrum of panel (a) is repeated in (e) with a blue (grey) line as reference.

The period of the slow oscillation of the average displacement $\langle x(t)\rangle_{\rm KH}$ is approximately twice as large as the modulation period. This is because

$$\begin{aligned}\langle x(t)\rangle &\equiv \langle\psi|x|\psi\rangle \approx c_g^*(t)c_{e_1}(t)\langle g|x|e_1\rangle \\ &\sim c_g^*(t)c_{e_1}(t)\exp\left[i\left(\varepsilon_g - \varepsilon_{e_1}\right)t\right],\end{aligned} \tag{8}$$

where $|\psi\rangle \approx c_g(t)|g\rangle + \sum_{i=1}^4 c_{e_i}(t)|e_i\rangle$, with the ground state $|g\rangle$ and excited bound states $|e_i\rangle$, and neglecting the small contribution of the continuum states. The period of the slow oscillation of $\langle x(t)\rangle_{\rm KH}$ is determined by the energy difference $\varepsilon_{e_1} - \varepsilon_g$, which is almost twice as small as $\varepsilon_{e_2} - \varepsilon_g$ [the fast oscillation of $\langle x(t)\rangle_{\rm KH}$ is due to $c_g^*(t)c_{e_1}(t)$]. Thus, the energy levels of the KH states are approximately equidistant, corresponding to the drift period T_d, $|\varepsilon_g - \varepsilon_{e_1}| \approx 2\pi/T_d$. The enhancement of the ionization happens twice during the drift period $\Delta t = T_d/2$, which determines the separation of the fine peaks in the spectral line $\Delta\varepsilon = 2\pi/\Delta t \approx 2|\varepsilon_g - \varepsilon_{e_1}| \approx |\varepsilon_g - \varepsilon_{e_2}|$.

A question arises as to why the peak corresponding to the ionization from the first excited state is absent in the ATI spectrum. Is this bound KH state not populated during the ramp of the laser pulse? In fact, the population of this state is responsible for the average coordinate oscillation $\langle x(t)\rangle_{\rm KH}$ and, therefore, it does exist. If there were contributions to the ionization WP from the first excited state, the WP would have

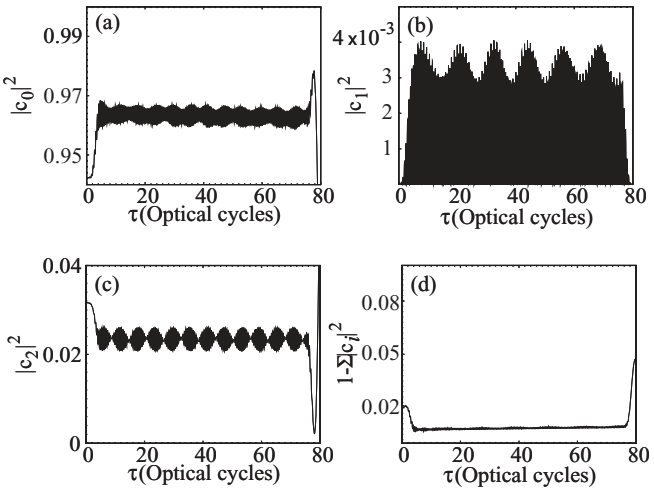

FIG. 6. (a), (b), (c) The time profiles of the population dynamics of the bound KH states and (d) the population dynamics of the continuum states in the laser field. The ionization increases smoothly during the interaction with the laser pulse. The laser parameters are the same as in Fig. 4.

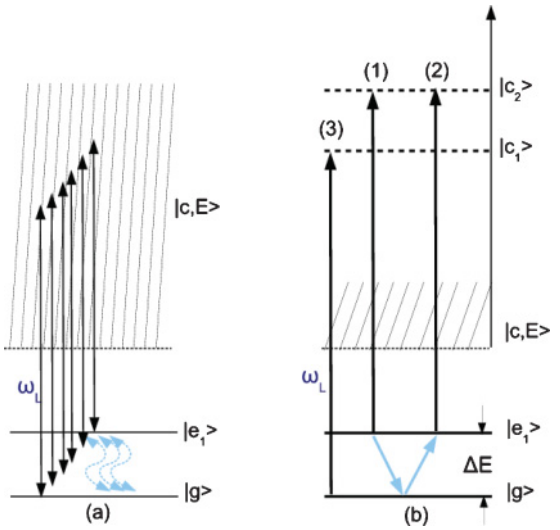

FIG. 7. (Color online) (a) Schematic energy-level diagram: two adjacent light-induced bound states $|g\rangle, |e_1\rangle$ are coupled to a common continuum $|c, E\rangle$, which results in the Raman transitions and coherent population transfer between the bound dressed states. (b) Schematic for interfering ionization paths (1) and (2). The pathway (2) is mediated via Raman coupling as indicated in subfigure (a) [blue (gray) arrows]. Compared with the ATI spectra of Figs. 5(a) and 5(b), the first peak corresponds to the path (3), direct ionization from the ground state, and the second peak corresponds to the transition from the third bound state to continuum, which is not shown in (b).

a modulation component with a period twice as large. As the modulation of the ionized WP and its period is induced by the drift motion of the bound WP, therefore, one may expect that the suppression of the ionization from the first excited state should also be connected with the drift. To address this question, we investigate the population dynamics of the bound states in the laser field; see Fig. 6. First of all, we see in Fig. 6(b) that the population of the first excited state does not vanish and, in principle, could have produced an ionization peak in the ATI spectrum. With increasing of the laser intensity, the field-free bound state evolves into the bound and continuum light-induced states. During the ramp of the laser pulse, mainly the states with the same parity as the initial state are populated without photon absorption. Later, during the flat part of the laser pulse, the dressed bound states couple to each other via the continuum due to photon absorption, which results in oscillations of the state populations. In this way, the states with different parity from the initial one can be populated during the interaction with the laser pulse, for example, the first excited state; see Fig. 6(b). The population in the first excited KH state shows six oscillations on the envelope during the constant part of the pulse, similar to the ionization WP [see Figs. 6(b) and 4], which are correlated with the minima of $\langle x(t)\rangle_{\mathrm{KH}}$, that is, with the electron drift motion. Thus, the population of the first excited KH state is enhanced due to the drift motion of the bound WP, inducing a coupling between the ground and the first excited states. The latter increases the contribution of the negative-parity bound states, necessary for the formation of the very asymmetric bound WP at the turning points of the drift motion.

Due to the coupling of the bound KH states via continuum, there can be additional quantum paths for ionization besides the direct ionization path, creating interference effects in the ATI spectrum. Let us investigate the possibility for interference of different quantum paths to the continuum originating from different bound states. We have calculated the ATI spectrum by projecting out the population of either the ground KH state [Fig. 5(c)] or the first excited one [Fig. 5(d)] after the raising ramp of the laser pulse. In the first case, when the ground-state population is projected out, the ionization path starting from this state is canceled (the peak corresponding to the ionization from the ground state disappears), as one expects. At the same time, it is remarkable that the peak related to the first excited KH state appears in this case. This indicates the existence of the direct ionization path from the first excited KH state to the continuum; see path 1 in Fig. 7(b). However, there is another ionization path originating from the first excited state due to Raman stimulated coupling of the ground and the first excited states, shown in Figs. 7(a) and 7(b) by blue (grey) arrows. It proceeds to continuum via the ground state; see the path 2 in Fig. 7(b). In the second case [see Fig. 5(d)], there is no initial population in the first excited KH state. However, surprisingly, the peak corresponding to ionization from this first excited state still persists, along with the expected peak from the ground state. This is because of not-stimulated population transfer from the ground state to the first excited one [only an upward blue (grey) arrow in Fig. 7(b)]. One can conclude from these results that an additional path exists to the continuum which originates from the first excited state proceeding to the ground state and further to the continuum. Thus, there are two interfering paths ending up at the same continuum state: (1) direct transition from the first excited KH state to the continuum and (2) transition from the first excited KH state to the ground state and further to the continuum; see Fig. 7. The interference between the mentioned two paths to the continuum is destructive as it suppresses the ionization peak corresponding to the ionization from the second KH state; see Figs. 5(a) and 5(b). Note

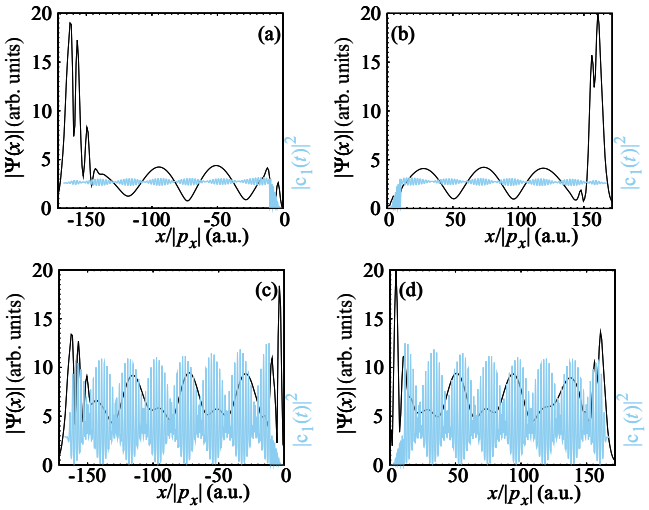

FIG. 8. (Color online) (black) The time profile of the ionization probability of the electron WP of a 1D model atom $\varepsilon = 4\omega$ and $\sigma = 1$. [blue (grey)] The time variance of the population on the second KH state: (a) and (b) for the system from which the first KH state after the ramp is projected out; (a) negative and (b) positive direction. In panels (c) and (d) the second KH state after the ramp is projected out. The peak electric field is $E_0 = 25.0$, and the laser frequency is $\omega = 3$ a.u.. In (a) and (c), the time is reversed for population dynamics.

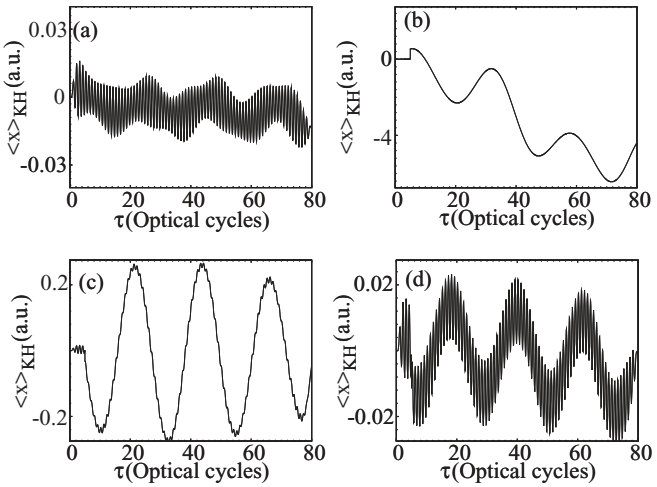

FIG. 9. The expectation value of the electron displacement of a model atom irradiated by a laser pulse of frequency $\omega = 3$ a.u. and electric field $E = 25$ a.u. in the KH frame: (a) no state is projected out and (b) first KH state, (c) second KH state, and (d) third KH state are projected out.

that this interference is different from the one in the regime of the interference stabilization of Rydberg atoms [30]. In the interference stabilization regime, the different paths to the continuum from the different close-lying Rydberg states interfere because the bandwidth of the energy levels exceeds the level spacing, resulting in the complete suppression of ionization. In the considered case, the levels are well separated and the interference suppresses only the ionization from the specific KH state. In the interference stabilization regime, the interference is the cause of the stabilization, while in the considered case the stabilization is a precondition to observe the interference effect in ATI spectra.

In order to clarify the other possible couplings between bound dressed states, the third KH state is projected out after the raising ramp and the ATI spectra at the end of the pulse is calculated and compared with the complete spectrum in Figs. 5(e) and 5(f). This figure shows no other interference signature.

In the last part of this section, we discuss how the changes of the fine structure of the spectral line, when some bound states are projected out after the ramp of the laser pulse (see Fig. 5), can be explained using the details of the modified drift motion and the bound-state population dynamics. Removing the population of one of the coupled bound states after the ramp of the laser field changes the time profile of ionization. The time profile of the ionized WP with energy 4ω corresponding to the same peak in Fig. 5(a) for the case that the ground state is projected out, shown in Fig. 8(a), and compared with the time profile of the population in the second KH states. The ionization in the negative direction of the box is shown in (a) and in the positive direction is shown in (b). One can see that the number of oscillations within the envelope of the time profile of the WP is half of that of Fig. 4, while the oscillation of the population of the first excited state is the same with different amplitude and form. The phase of modulation of the ionization WP moving left is shifted by π with respect to that of right, in contrast to the case when all dressed bound states are contributing; see Fig. 4. When the ground-state population is removed after the ramp, the contribution to the ionized WP comes from the first and second excited states according to the spectrum; that is, in Eq. (7) $a_1 = \langle p|S|e_1\rangle$, $a_2 = \langle p|S|e_2\rangle$, and $\Delta\varepsilon = \varepsilon_{e_2} - \varepsilon_{e_1}$. The latter $\Delta\varepsilon$ is almost twice as small as $\varepsilon_{e_2} - \varepsilon_g$, which is the reason of the increase of the modulation period in Fig. 8. The phase shift between the ionized wave packet moving right and left is due to the π-phase shift of the $\Delta\varphi$ in Eq. (7) at the coordinate inversion because of the difference in parity of $|e_1\rangle$ and $|e_2\rangle$. When the first excited state is removed after the ramp, the contribution to the ionized WP comes from the ground state and the first and second excited states (see Fig. 5); the largest ones are $a_1 = \langle p|S|g\rangle$ and $a_2 = \langle p|S|e_1\rangle$. Accordingly, the modulation period again is almost twice as large, and there is a π-phase shift at the coordinate inversion.

Moreover, we observe the following correlation between the drift motion and the enhancement of the ionization in the case when projecting out some of the bound states. When the WP drifts to one side, the ionization in the same side is larger than in the opposite side at the same moment. This can be explained by inspecting the variation of the expectation value of the electron displacement; see Fig. 9. While the displacement is small at the turning points when no states are projected out ($\langle x\rangle_{\rm KH} \approx 0.01$ a.u.), it is rather large when some states are projected out [$\langle x\rangle_{\rm KH} \approx 2$ a.u. in (b) or 0.2 a.u. in (c)]. This can be the cause of the left-right asymmetry of the ionization WP in Fig. 8. However, the population transfer between the bound states happens with the same probability irrespective of the drift direction. Consequently, the number of oscillations of the envelope of the ionization WP on each side is half of the oscillation of the population of the bound state. At last, the fast oscillation in Figs. 9(a) and 9(d), which

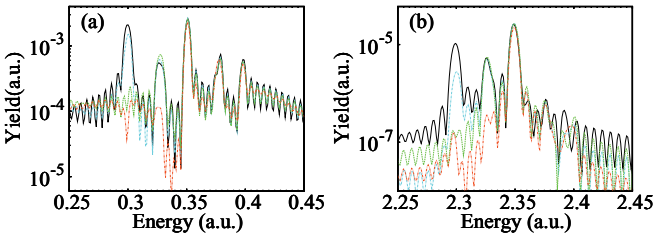

FIG. 10. (Color online) (a) First and (b) sixth peaks in the ATI spectra of the model atom irradiated with a 80-cycle laser pulse with $E_0 = 2.4$ and $\omega = 0.4$. The black line denotes all KH states included in the interaction within the flat part of the pulse, the dot-dashed (blue) line denotes the first KH state, the dashed (green) line denotes first and second KH states, and the double dot-dashed (red) line denotes the first and third KH states are projected out.

is mainly due to the coupling of the first two KH states with different parities, is vanished in (b) and (c) by projecting out one of them. The time profile of the ionized WP with energy 4ω corresponding to the same peak in Fig. 5(b), for the case in which the second KH state is projected out, is shown in Figs. 8(c) and 8(d) and compared with the time profile of the population of the second KH state. The relation between the number of the oscillations of the envelope of the time profile of the WP and oscillations of the population of the second light-induced state is similar to Fig. 8(a).

V. THE CASE OF LOW-FREQUENCY STABILIZATION

In this section, we shortly discuss the considered effects of the drift, the bound population transfer, and the interference in the ATI spectrum at intermediate frequencies $\omega \lesssim I_p$ when stabilization can still take place. The ATI spectra (spectral lines corresponding to single- and six-photon process) for a model atom irradiated by a laser pulse with $\omega = 0.4$ and $E_0 = 2.4$, which is in the stabilization regime, are shown in Fig. 10. The peak positions correspond to the energies of the KH states; the latter is indicated in Table I. Note that the first peak results from the first two bound states as their energies are very close.

There is no distinct destructive interference, as in the high-frequency case. However, one can see the trace of this interference in the second peak of Figs. 10(a) and 10(b), noting the enhancement of the peak when projecting out of the first two bound states. That latter means that the coherent population transfer is inefficient in the low-frequency case. The time profile of the ionized WP is calculated and shown in Fig. 11. There is enhancement of the ionization, but they are decreasing in amplitude and are rather irregular. These features are probably connected with the higher ionization rate in the low-frequency case, a large drift of the WP to one side during the rising ramp, and comparable contributions to

TABLE I. Energy levels of the KH states interacting with a laser pulse of $\omega = 0.4$ and $E_0 = 2.4$.

n	Energy (a.u.)	n	Energy (a.u.)	n	Energy (a.u.)
0	-1.033×10^{-1}	2	-7.348×10^{-2}	4	-2.449×10^{-2}
1	-1.021×10^{-1}	3	-5.215×10^{-2}	5	-2.745×10^{-3}

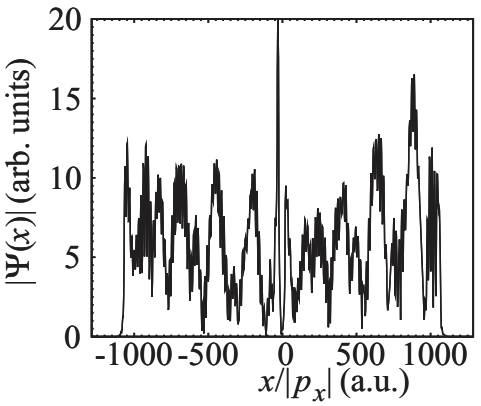

FIG. 11. Time profile of the ionized WP with energy $\varepsilon = 4\omega$ for the same system as in Fig. 10, $\sigma = 0.3$ a.u..

the ionization WP from many bound states. The population dynamics is shown in Fig. 12. From this figure, the trace of the drift-induced population transfer can be seen, which, however, is decreased in amplitude and is irregular, similar to the ionization behavior of the WP.

VI. CONCLUSION

We have studied the time structure of the ionization dynamics of a model atom in the stabilization regime in a laser field of low and high frequencies. We find direct connections among the drift of the bound WP in the KH frame, the modulation of the ionized WP, the population dynamics of the dressed bound states, and the interference effect in the spectral lines. At the turning points of the drifting bound WP, the electron velocity is low, the Coulomb field influence is large, and photon absorption is enhanced. Due to the latter, the ionization probability is periodically enhanced in each half period of the drift motion. With the same periodicity, transitions from the bound state to the excited states are

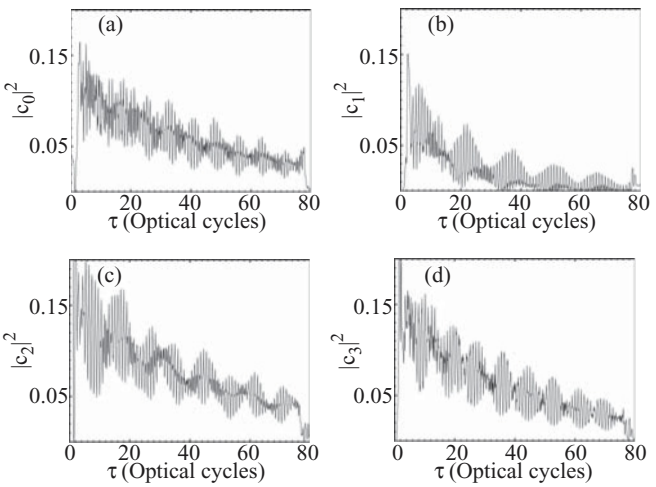

FIG. 12. Time profile of the population dynamics of the bound KH states. The peak electric field is $E_0 = 2.4$, the laser frequency is $\omega = 0.4$ a.u. and the pulse length is 80 optical cycles including a 5-cycle ramp.

induced. The coherent population transfer between the dressed bound states creates additional paths to the continuum, which results in the suppression of the ionization from the first excited KH state. The mentioned effect is clearly exhibited in the high-frequency case. It does still exist in the low-frequency domain of the stabilization regime but is obscured by contributions to the ionizing WP from many bound states and is decreased due to the high ionization rate.

[1] P. Agostini and L. F. DiMauro, Rep. Prog. Phys. **67**, 813 (2004).

[2] [http://hasylab.desy.de/facilities/flash/] [http://lcls.slac.stanford.edu/] and [http://www-xfel.spring8.or.jp/].

[3] Employing typical FLASH parameters with photon energy $\omega \sim 100$ eV and laser intensity 10^{16} W/cm^2, we obtain as ATI parameter $U_p/\omega \sim 3 \times 10^{-3}$, Keldysh parameter $\gamma = \sqrt{I_p/2U_p} \sim 10$, and stabilization parameter $\alpha = E_0/\omega^2 \sim 0.06$, which indicates the perturbative regime where $U_p = E_0^2/4\omega^2$ is the ponderomotive potential, E_0 is the laser field, and $I_p \sim 1$ is the ionization potential.

[4] In particular, when using seeded XFEL or high-order harmonic generation from overdense plasma surface. See e.g., G. Lambert *et al.*, Nature Phys. **4**, 296 (2008); B. Dromey *et al.*, *ibid.* **5**, 146 (2009).

[5] N. Miyamoto, M. Kamei, D. Yoshitomi, T. Kanai, T. Sekikawa, T. Nakajima, and S. Watanabe, Phys. Rev. Lett. **93**, 083903 (2004).

[6] H. Hasegawa, E. J. Takahashi, Y. Nabekawa, K. L. Ishikawa, and K. Midorikawa, Phys. Rev. A **71**, 023407 (2005).

[7] H. Wabnitz *et al.*, Nature (London) **420**, 482 (2002).

[8] A. A. Sorokin, S. V. Bodashev, T. Feigl, K. Tiedtke, H. Wabnitz and M. Richter, Phys. Rev. Lett. **99**, 213002 (2007).

[9] R. Santra and C. H. Greene, Phys. Rev. A **70**, 053401 (2004).

[10] S. Bauch and M. Bonitz, Phys. Rev. A **78**, 043403 (2008).

[11] M. Pont and M. Gavrila, Phys. Rev. Lett. **65**, 2362 (1990).

[12] M. Gavrila, *Atoms in Intense Laser Fields* (Academic, New York, 1992).

[13] H. A. Kramers, *Collected Scientific Papers* (North-Holland, Amsterdam, 1956), p. 272; W. C. Henneberger, Phys. Rev. Lett. **21**, 838 (1968).

[14] Q. Su, J. H. Eberly, and J. Javanainen, Phys. Rev. Lett. **64**, 862 (1990).

[15] M. Gavrila, J. Phys. B **35**, R147 (2002).

[16] M. Gavrila, I. Simbotin, and M. Stroe, Phys. Rev. A **78**, 033404 (2008); M. Stroe, I. Simbotin, and M. Gavrila, *ibid.* **78**, 033405 (2008).

[17] This condition adjusts the usual condition for HFFT and for the stabilization regime. The usual condition assumes that the laser frequency is larger than the energy of a bound state in the Kramers-Henneberger potential $\Delta\varepsilon \sim 1/\alpha^2$, which yields $\alpha\sqrt{\omega} \gg 1$; see M. Gavrila and J. Z. Kaminski, Phys. Rev. Lett. **52**, 614 (1984).

[18] H. Miyagi and K. Someda, Phys. Rev. A **80**, 023416 (2009); **82**, 013402 (2010).

[19] Z. Zhou and J. Yuan, Phys. Rev. A **77**, 063411 (2008).

[20] K. Toyota, O. I. Tolstikhin, T. Morishita, and S. Watanabe, Phys. Rev. A **76**, 043418 (2007).

[21] K. Toyota, O. I. Tolstikhin, T. Morishita, and S. Watanabe, Phys. Rev. Lett. **103**, 153003 (2009).

[22] K. Z. Hatsagortsyan *et al.*, J. Opt. Soc. Am. B **25**, 93 (2008).

[23] C. H. Keitel and P. L. Knight, Phys. Rev. A **51**, 1420 (1995).

[24] H. Ebadi and H. Sabzyan, J. Iran. Chem. Soc. **6**, 489 (2009).

[25] R. S. Varga, *Matrix Iterative Analysis* (Prentice-Hall, Englewood Cliffs, NJ, 1962).

[26] K. J. Schafer and K. C. Kulander, Phys. Rev. A **42**, 5794 (1990).

[27] D. Bauer, Phys. Rev. Lett. **94**, 113001 (2005).

[28] R. Grobe and C. K. Law, Phys. Rev. A **44**, R4114 (1991).

[29] Note that due to a large ionization background at low energy, this deep is not clearly distinguishable at the first ATI peak.

[30] M. V. Fedorov and A. M. Movsesian, J. Opt. Soc. Am. B **6**, 928 (1989); M. V. Fedorov, Quantum Electron. **29**, 578 (1999); *Atomic and Free Electrons in a Strong Light Field* (World Scientific, Singapore, 1997), p. 452.